BILINGUAL PUBLISHING GROUP

Journal of Building Material Science

https://journals.bilpubgroup.com/index.php/jbms/index

ARTICLE

Numerical Study of GFRP-reinforced Concrete Beams with Straight and Hooked-end Bar Lap Splices

***Sara Mirzabagheri*[1], *Osama (Sam) Salem*[2*]**

[1] *Civil Engineering Division, Islamic Azad University, Parand Branch, Parand, 3761396361, Iran*

[2] *Department of Civil Engineering, Faculty of Engineering, Lakehead University, Thunder Bay, ON P7B 5E1, Canada*

ABSTRACT

Glass fibre-reinforced polymer (GFRP) has been increasingly used as the main reinforcement in concrete structures due to its durability and resistance to corrosion. However, there is a lack of data regarding the bond behaviour of GFRP bars with 180-degree hooked ends used in flexure concrete elements. To investigate the effects of the hooked ends of GFRP bars on the bond strength with concrete, beams reinforced with GFRP bars with straight and hooked-end lap splices at the midspan were modelled using ABAQUS/Standard software. The finite element models were validated using the experimental results of four full-size concrete beams. Two beam specimens had straight-end bars, while the other two had hooked-end bars. Sensitivity analysis was performed to find the proper values for model verification, such as dilation angle and mesh density. According to the outcomes of the parametric study conducted in this research, changing the length of the bar lap splices in the range of 15 to 40 times the bar diameter had a negligible effect on the beam's overall behaviour. Increasing the number of reinforcing bars from 3 to 5 increased the beam flexural strength by about 33%, whereas increasing the diameter of the bars from 10 to 20 mm doubled the beam strength.

Keywords: Concrete beams; GFRP reinforcing bars; Bar lap splice; Straight-end bars; Hooked-end bars; GFRP-concrete bond strength

1. Introduction

Corrosion is a phenomenon that considerably decreases the service life of concrete structures. To remedy this issue, new materials have been produced

*CORRESPONDING AUTHOR:
Osama (Sam) Salem, Department of Civil Engineering, Faculty of Engineering, Lakehead University, Thunder Bay, ON P7B 5E1, Canada; Email: sam.salem@lakeheadu.ca

ARTICLE INFO
Received: 21 December 2023 | Revised: 12 March 2024 | Accepted: 15 March 2024 | Published Online: 1 April 2024
DOI: https://doi.org/10.30564/jbms.v6i1.6170

CITATION
Mirzabagheri, S., Salem, O.S., 2024. Numerical Study of GFRP-reinforced Concrete Beams with Straight and Hooked-end Bar Lap Splices. Journal of Management Science & Engineering Research. 6(1): 1–16. DOI: https://doi.org/10.30564/jbms.v6i1.6170

to survive in harsh environmental conditions. Glass fibre-reinforced polymer (GFRP) bars have been used as a substitute for conventional steel rebar in concrete structures due to its advantages, such as corrosion resistance and high strength-to-weight ratio compared to steel rebar. For high importance concrete structures such as dams, bridges, and power plants, GFRP is an ideal reinforcing material alternative [1]. The bond of GFRP bars to concrete was experimentally tested using pull-out tests, which included 90-degree hooked-end bars. Design guidelines were derived from the results of these tests for bonding between GFRP bars and concrete [2]. In another study conducted by Morphy, 113 concrete panel specimens were tested to determine the losses of FRP stirrup capacity, and recommendations were made for utilizing FRP stirrups [3]. The long-term behaviour of GFRP bars was reported by Ehsani, et al [2], where the residual strength and modulus of elasticity of GFRP bars embedded in concrete were evaluated over a duration of seven years. In addition, a computer model was developed as part of that study, and it showed that the decrease of bar strength was faster over the first few years of the study time span [1]. Another study conducted by Yang et al. involved steel, CFRP and GFRP bars that were used in small-size concrete beams to investigate the influence of adding fibres to concrete on the load-carrying capacity of the beams made of high-strength concrete. It was noticed that adding fibres increased the ultimate flexural strength and ductility of the specimens [4]. The near-surface mounted (NSM) method is a technique that has emerged to enhance the capability of using FRP. In the NSM technique, FRP bars or laminates are embedded into pre-cut grooves on the concrete cover of reinforced concrete beams. In 1999, a few researchers proposed using NSM FRP rods to rehabilitate RC beams [5,6]. An epoxy paste adhesive significantly increases the bond strength between the FRP reinforcement and concrete because the FRP materials are surrounded on three sides [7,8]. In addition, several studies have been conducted to develop numerical and analytical bond-slip models for NSM FRP-concrete joints, such as those conducted by De Lorenzis and La Tegola [9] and Yuan et al. [10]. In a study by Sharaky et al. [11], concrete beams strengthened with NSM FRP bars were experimentally examined. In their study, the concrete beams were subjected to four-point flexural bending. The outcomes of that experimental study showed that the beams strengthened with CFRP bars had greater stiffness than those strengthened with GFRP bars [11]. A study on the compressive behaviour of GFRP bars in concrete cylinders proved that GFRP bars had the capability of withstanding high levels of compressive strains long after reaching the peak load of the specimens without any premature crushing [12].

Various researchers did numerical modelling of reinforced concrete structures because of its power in studying various types of structures [13,14]. However, it is strongly suggested that experimental results be used to validate computer models and then the validated models be used to simulate the behaviour of structures. Following such a strategy enables the investigation of specific factors that are often difficult to investigate through experiments more efficiently and cost-effectively. Besides experimental investigations, a few researchers conducted numerical studies of concrete structures reinforced with FRP bars. For instance, Yang studied the behaviour of concrete beams reinforced with continuous FRP bars through experimental and numerical investigations. That study aimed to better understand the deformation behaviour of the tested beams. Also, the numerical study revealed a new approach to model the development of shear resisting truss mechanism and to estimate the inclination of the developed compressive forces within the concrete beams [15]. Stoner modelled twelve concrete beams with and without GFRP stirrups using ABAQUS/Standard software, and the outcomes of the developed model agreed with those of the models developed in similar studies. In Stoner's model, truss and membrane elements were used to model the reinforcing bars [16].

In another numerical study on the behaviour of reinforced concrete beams conducted by Roudsari et al., steel, CFRP, and GFRP bars were used in the modelled specimens. It was concluded that the beams

with GFRP bars had greater mid-span deflections than those of other beams [17]. Prediction of the response of GFRP-reinforced concrete columns under concentric and eccentric axial loads was modelled using ABAQUS/Standard software by Elchalakani. The model's outcomes were verified against experimental test results, where the predicted N-M strength interaction diagrams had good agreement with the experimental results [18]. In another numerical study, GFRP-reinforced concrete columns were modelled to investigate parameters such as the load-carrying capacity of the columns, longitudinal reinforcement ratio and compressive strength of concrete. Good agreement was seen between the numerical predictions and experimental results [19].

Research on the bond of spliced FRP bars as reinforcement of flexure concrete members is limited. A study by Aly et al. [20] tested twelve concrete beams reinforced with spliced CFRP bars. The effects of bar diameter and splice length on bond strength were investigated. Results show that the FRP stress limit was directly proportional to the splice length [20]. In another experimental study, thirteen beam specimens were tested to investigate the bond strength of lap spliced GFRP bars [21]. It was seen that the effect of transverse reinforcement on the bond strength between GFRP bars and concrete depends on the surface properties of reinforcing bars. In a more recent study, twenty-two beams with FRP bars were experimentally tested to investigate the effects of parameters such as the spacing of stirrups along the bar splice length, bar diameter, loading type, and type of spliced bar [22]. It was concluded that stirrups along the splice length increased the bond strength of GFRP bars. Most recently, eight full-scale GFRP-reinforced concrete beams with reduced spacing of shear stirrups were tested [23]. Results show that the bond performance of GFRP bars was enhanced with the reduction in shear stirrups' spacing in the lap zone.

Nevertheless, no sufficient data exists on the bond strength of 180-degree hooked-end GFRP bars with concrete in a full beam test setup. One of the very few studies conducted in this regard is an experimental study by Nour et al. [24] on four full-size concrete beams with mid-span bar lap splices. Two configurations were used for reinforcing lap splices; two beam specimens had straight-end bar lap splices, while the other two had 180-degree hooked-end bar lap splices. All beam specimens were subjected to four-point flexural bending until failure. Experimental results show that the 180-degree hooked-end GFRP bars had considerably stronger anchorage with concrete than straight-end bars, ultimately increasing the flexural strength and stiffness of the tested concrete beams [24].

Due to the lack of experimental data on the behaviour of full-size concrete beams reinforced with FRP bars, numerical studies can be highly beneficial in investigating various aspects of beam reinforcement, including bar end configurations (e.g., straight, hooked, etc.) and bar diameter and number. Accordingly, for the study presented in this paper, ABAQUS/Standard was utilized to simulate the behaviour of full-size concrete beams reinforced with GFRP bars with mid-span lab splices. Three-dimensional eight-node solid elements (C3D8R) were used for all reinforcing bars and concrete to achieve the best results. Sensitivity analyses were performed to determine the most efficient model regarding mesh density, dilation angle, and viscosity parameters. After successful validation of the developed FE model against the experimental results obtained from the study conducted by Nour et al. [24], a parametric study was completed to investigate the effect of the number and diameter of GFRP bars, as well as the effect of the splice length on the overall behaviour of the reinforced concrete beams. In addition, the material of the reinforcing bars was changed to compare the behaviour of the beam with the same reinforcement configurations, e.g., bar diameter and number, but with a different material such as conventional steel.

2. Finite element models description and details

In this section, the methods used to obtain the results in the paper are elucidated. This allows readers to replicate the study in the future.

2.1 Solution strategy

ABAQUS software is a powerful tool for the numerical modelling of various structures. This software has an implicit/standard solver for linear/nonlinear static problems and an explicit solver for dynamic/large deformation problems. Implicit FEA can be used for most common engineering problems but requires considerable computation and accurate calculations to devise a solution. In nonlinear implicit analysis, the solution of each step requires a series of trial solutions (iterations) to establish equilibrium within a certain tolerance. No iteration is required in explicit analysis as the nodal accelerations are solved directly. Explicit FEA can generate faster solutions to most complex problems but typically requires expert software and skills to implement successfully. The explicit solution is more useful for reinforced concrete structures because of its merits in analyzing brittle materials and ease of convergence. Unlike the implicit solution, the explicit solution does not involve a global stiffness matrix for the modelled structure or assembly. Accordingly, the explicit dynamic solver of ABAQUS was used in this study.

2.2 Material properties

Three constitutive models are included in ABAQUS software, i.e., the Smeared Crack Model (SCM), Brittle Cracking Model (BCM) and Concrete Damaged Plasticity Model (CDPM). In CDPM, both tensile cracking and compressive crushing are considered. Isotropic tensile and compressive plasticity and scalar isotropic damaged elasticity are used in this model. So, irreversible damage that occurs during the fracture process is considered by implementing the Concrete Damaged Plasticity Model in this study. To improve the convergence rate, the viscosity parameter was implemented in the FE models of this study.

In the plastic-damage concrete model, two equations, yield function and flow potential, are solved. equations (1) and (2) show the yield function and flow potential, respectively.

$$F = \frac{1}{1-\alpha}(\bar{q} - 3\alpha\bar{p} + \beta(\tilde{\varepsilon}^{pl})\left\langle\hat{\bar{\sigma}}_{\max}\right\rangle - \gamma\left\langle-\hat{\bar{\sigma}}_{\max}\right\rangle) - \bar{\sigma}_c(\tilde{\varepsilon}_c^{\,pl}) = 0 \tag{1}$$

$$G = \sqrt{\in \sigma_{t0}\tan\psi)^2 + \bar{q}^2} - \bar{p}\tan\psi \tag{2}$$

where,

$$\bar{p} = -\frac{1}{3}\bar{\sigma} : \mathrm{I} \tag{3}$$

$$\bar{q} = \sqrt{\frac{3}{2}\bar{S} : \bar{S}} \tag{4}$$

$$\bar{S} = \bar{p}I + \bar{\sigma} \tag{5}$$

$$\alpha = \frac{(\sigma_{b0}/\sigma_{c0}) - 1}{2(\sigma_{b0}/\sigma_{c0}) - 1}; 0 \le \alpha \le 0.5 \tag{6}$$

$$\beta(\tilde{\varepsilon}^{pl}) = \frac{\bar{\sigma}_c(\tilde{\varepsilon}_c^{\,pl})}{\bar{\sigma}_t(\tilde{\varepsilon}_t^{\,pl})}(1-\alpha) - (1+\alpha) \tag{7}$$

$$\sigma_{b0}/\sigma_{c0} \qquad \gamma = \frac{3(1-K_c)}{2K_c - 1} \tag{8}$$

Default values of 0.1, 1.16 and 0.667 are used for ∈, σb0 /σc0 , and K_c, respectively, as per the ABAQUS Theory Manual [25]. Proper values of the dilation angle and viscosity parameter were obtained through sensitivity analyses.

To model concrete's uniaxial stress-strain tension behaviour, a tension stiffening model was used to have the effect of dowel action and bond between bars and concrete. Accordingly, the Maekawa tension stiffening model [26] was utilized, and equation (9) was used to determine the tensile stiffening stress.

$$\sigma_t = f_t(\frac{\varepsilon_{tu}}{\varepsilon})^c \; for \varepsilon > \varepsilon_{tu} \tag{9}$$

where, f_t, ε_{tu}, ε, and c are uniaxial tensile strength, cracking strain, average tensile strain, and stiffening parameter, respectively. In equation (9), c equals 0.4 for deformed bars, and 0.2 for welded wire mesh reinforcement. **Figure 1** shows the tension stiffening model of Maekawa et al. [26].

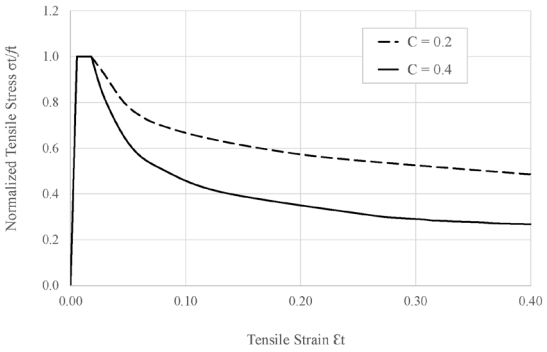

Figure 1. Tension stiffening model.

Source: Maekawa et al. [26].

For the uniaxial compression behaviour of concrete, the model proposed by Eurocode 2 [27] was utilized in this study. Accordingly, Equation 10 was used to determine the uniaxial compressive stress of concrete in the model (**Figure 2**).

$$\sigma_c = \frac{3\varepsilon f_c}{\varepsilon_{c1}(2+(\frac{\varepsilon}{\varepsilon_{c1}})^3)} \; for \varepsilon \le \varepsilon_{c1\theta} \tag{10}$$

For the values of strain over $\varepsilon_{c1\theta}$, linear or nonlinear model is permitted in Eurocode 2 [28].

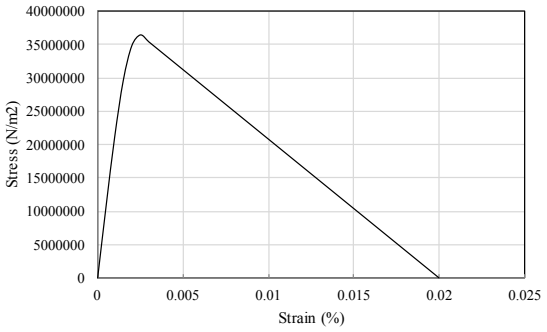

Figure 2. Uniaxial compression model.

In order to use metal plasticity model for steel bars, the simplified trilinear model was utilized as illustrated in **Figure 3**. Steel with 420 MPa strength and modulus of elasticity of 200,000 MPa was used.

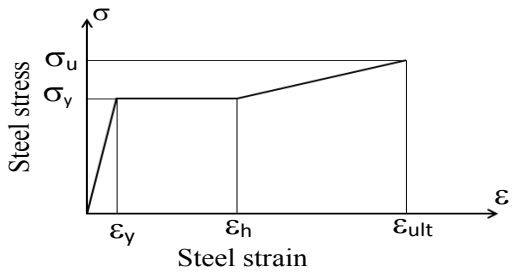

Figure 3. Simplified trilinear model for bars.

Source: Raza et al. [19].

Since GFRP has a brittle rupture mode of failure, both linear and elastic behaviour of this material was modeled until failure [16]. Moreover, the tensile strength of GFRP bars was set to 1250 MPa, based on the material data sheet provided by the manufacturer.

2.3 Element type

The ABAQUS element collection has a wide variety of elements, including shell, contact, beam, and hexahedral elements. The right element to use in a finite element model significantly depends on the application. Since precise finite element modelling of the experimentally tested concrete beams and detailed behaviour of GFRP bars were intended in this study, all parts were modelled with solid elements. Three-dimensional eight-node solid elements with reduced integration (C3D8R) were used for all the parts of the FE models developed in this study (i.e., concrete, steel stirrups, and GFRP bars). The C3D8R elements were chosen specifically for their capacity to express significant deformations and geometrical and material non-linearity. Compared to the standard eight-node solid elements with full integration (C3D8), C3D8R elements can produce more reliable results with no numerical difficulties, such as hourglassing or shear locking. For the beam modelled with straight-end bar lap splices, 3296 elements and 6231 nodes were used, while for those with hooked-end bar lap splices, 3488 elements and 6663 nodes were used.

2.4 Tested beams

Four full-size concrete beams, each reinforced with three GFRP bars with lap splices at the beam midspan, were experimentally tested in a prior study by Nour et al. [24]. Two of the beam specimens had straight-end bars, as shown in **Figure 4(a)**, while the other two specimens had hooked-end bars, as shown in **Figure 4(b)**, to investigate the bond strength between the GFRP bars and concrete at the beam midspan bar lap splice's location [24].

The average 28-day compressive strength of concrete was 36.4 MPa, and the elasticity modulus of GFRP bars provided by the supplier was 64.0 GPa. The two steel bars utilized at the top of the beam as stirrup hangers had a 10 mm diameter, while the three GFRP bars that formed the main reinforcement of the beam had a 20 mm diameter each. The overall length of the bar lap splices was 550 mm in both beam configurations. Each beam specimen was simply supported over two supports, one pinned and the other roller support, to avoid any axial thrust force that might develop in the beam at high loading levels. To maintain maximum moment values at the beam midspan where the bar lap splices existed and to avoid any shear force interference, a four-point flexural bending test was performed by applying load over two points on top of the beam at a loading rate of 2 kN/min as shown in **Figure 5**. This relatively low loading rate was deliberately applied to avoid premature cracks in the concrete beams. Experimental results show that all four specimens reached their respective theoretical design moment. However, the concrete beam specimens with hooked-end bar lap splices had stronger bar anchorage than the straight-end bar specimens. More details of the experimental results can be found in the study by Nour et al. [24].

2.5 FE models validation

Beam geometry was modelled in three dimensions using the ABAQUS/CAE interface. As previously mentioned, all parts of the beams were modelled using solid elements. **Figure 6** shows the reinforcement details as they were tested and modelled for beam specimens with straight and hooked-

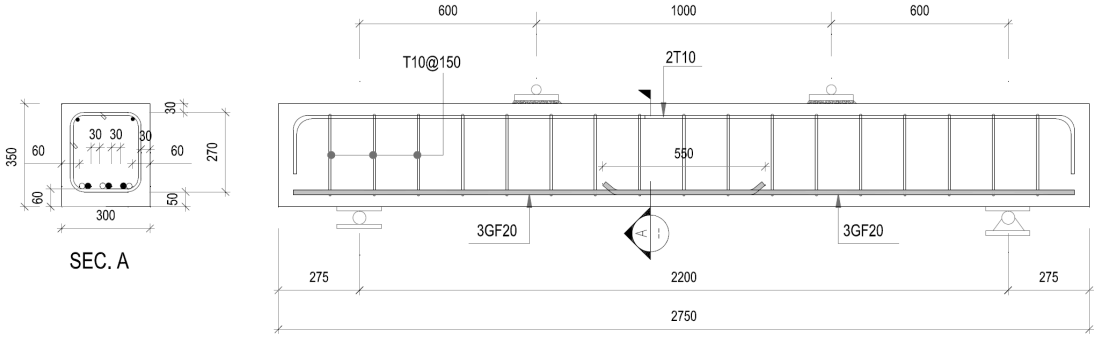

(a) Beam specimen with straight-end bar lap splices.

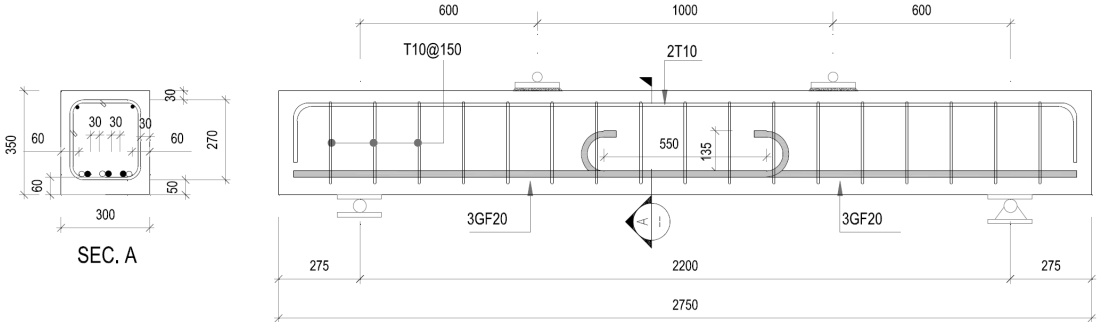

(b) Beam specimen with hooked-end bar lap splices.

Figure 4. Reinforcement details of the tested beams.

Source: Nour et al. [24].

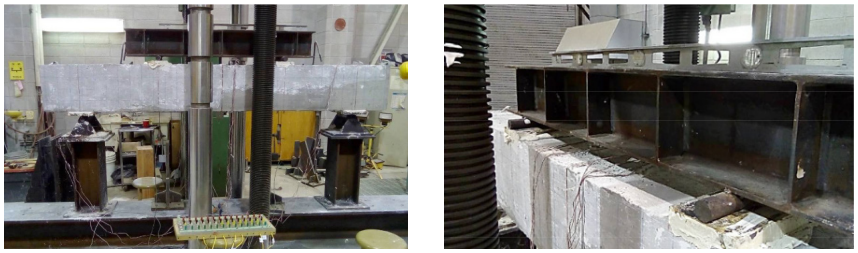

Figure 5. Test setup.

Source: Nour et al. [24].

end bar lap splices.

All material properties, details of reinforcement, and support conditions were modelled according to the details provided in the cited experimental study [24]. Monotonic loads were applied over two lines of nodes on top of the modelled beam, where the locations of applying load in experiments were rigid to those two reference lines. The locations of applied loads were the same in experiments and models. To achieve reliable outcomes, a series of sensitivity analyses were performed. Different mesh sizes, dilation angles, and viscosity parameters were studied, and their effects on the FE model results were analyzed.

The non-zero viscosity parameter can be used to improve the convergence of the model, but for larger values of this parameter, FE model results may be falsified. Sensitivity analysis of the viscosity parameter with the values of 0, 0.0001, and 0.01 showed no sensitivity of the FE model toward this parameter. Dilatancy is a phenomenon caused by shear in the microstructure of a material that induces an increase in its volume. Various dilatancy values were used for this parameter based on the coincidence of the results between numerical and experimental studies [28,29]. In the study presented in this paper, the dilation angle varied between 20 and 40 degrees (in 5-degree increments) to achieve the best results regarding the beam midspan deflections. As shown in **Figure 7** for beam specimens with straight and hooked-end bar lap splices, respectively, a dilation angle that equals 25 degrees led to the best results.

It is worth noting that for the GFRP bars, the mesh size was 40 mm, while for the steel stirrups and stirrup hanger bars, the mesh size was 100 mm. Also, the cross section of each of the GFRP bars, stirrups and stirrup hangers was partitioned into four equal quarters. To investigate the effect of concrete mesh size on the model results, mesh sizes that var-

(a) Experimental bar cage [24].

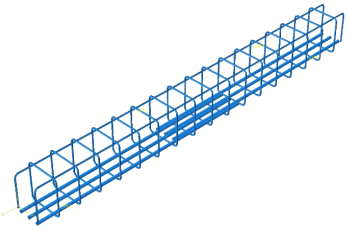

(b) Beam with straight-end bar lap splices.

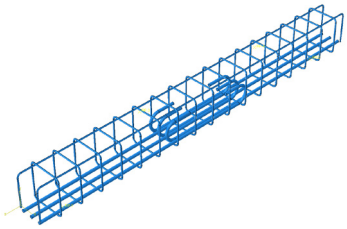

(c) Beam with hooked-end bar lap splices.

Figure 6. FE model reinforcement details.

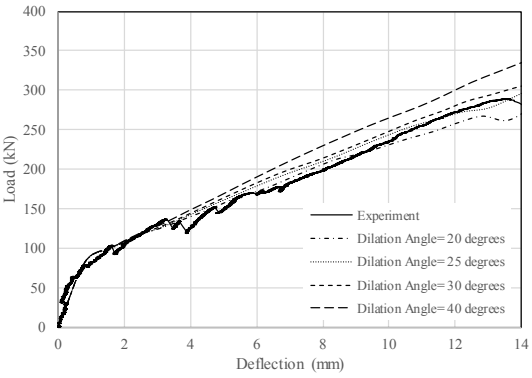

(a) Beams modelled with straight-end bar lap splices.

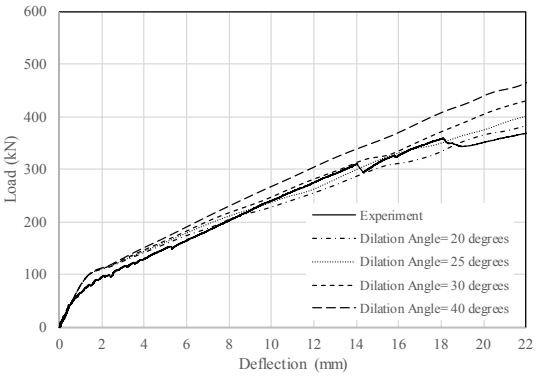

(b) Beams modelled with hooked-end bar lap splices.

Figure 7. Sensitivity analysis outcomes for the effect of the dilation angle.

ied between 40 and 80 mm (in 20-mm increments) were investigated. **Figure 8** illustrates the effect of concrete mesh size on the FE model outcomes regarding beam midspan deflections for beam specimens with straight and hooked-end bar lap splices, respectively.

As seen in **Figure 8**, three mesh sizes of 40, 60 and 80 mm were used in the modelling, and results were compared with the experiments. Stiffness, the slope of the diagram, was the same for the models with 60 mm mesh size and experiments. Strength, which is the ability to tolerate the applied loads, was also the same. So, concrete with a mesh size of 60 mm had the best agreement with the experimental results regarding strength, stiffness, and ductility.

Tensile stresses damages of straight and hooked-end bar beam models are presented in **Figure 9**, respectively. As shown in the figures, the cracking pattern of the beams was mainly vertical flexural cracks between the two loading points, followed by cracks between the support and the nearest loading point from either end of the beam. It is worth mentioning that **Figure 9** shows the tensile stresses damage contour at the last stage of applying the load, which concurred with the maximum beam midspan deflections that were greater in the beam model with hooked-end bar lap splices.

3. Parametric study

A parametric study using validated FE models has investigated the effect of the GFRP bar end configuration within the beam bar lap splices zone on the bar-concrete bond strength. Study parameters included the number and diameter of the reinforcing bars and the overall length of the beam bar lap splices.

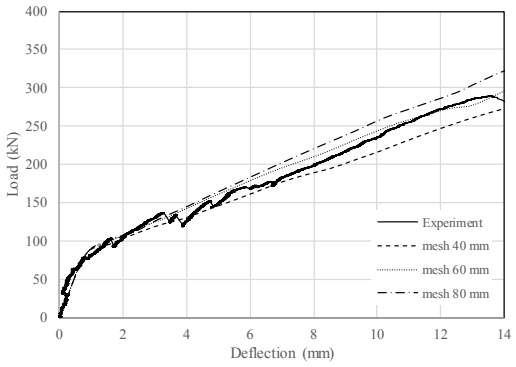

(a) Beams modelled with straight-end bar lap splices.

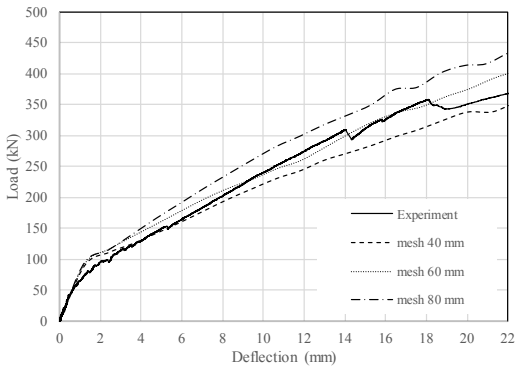

(b) Beams modelled with hooked-end bar lap splices.

Figure 8. Sensitivity analysis outcomes for the effect of concrete mesh size.

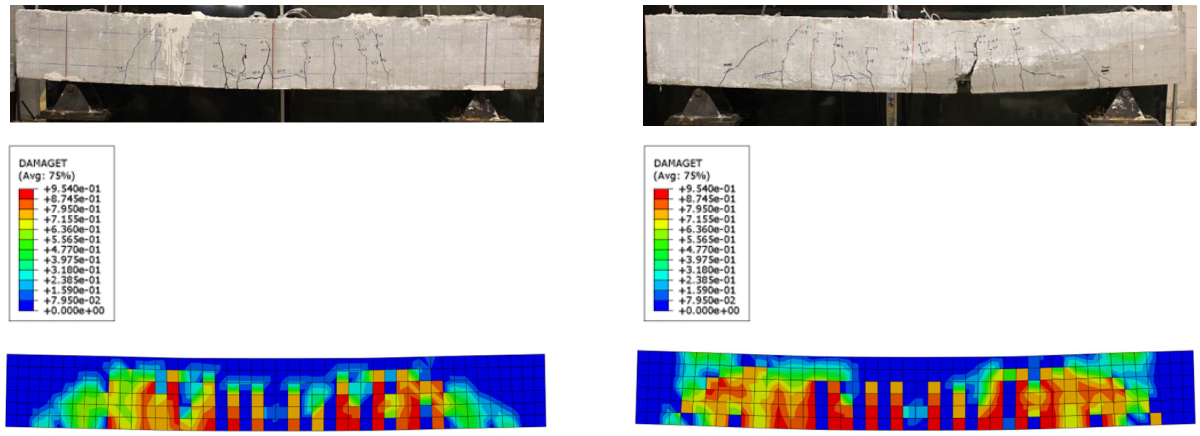

(a) Beam modelled with straight-end bar lap splices. (b) Beam modelled with hooked-end bar lap splices.

Figure 9. Tensile stresses damage contour.

3.1 Spliced versus continuous GFRP bars

Most of the experimental studies on the behaviour of GFRP-reinforced concrete beams in the literature utilized continuous bars [16,17]. So, GFRP bars were modelled continuously to compare the difference between the two reinforcement configurations in this study. In **Figure 10**, it is shown that although the initial stiffness of the beam with continuous bars was higher than that of the beams with either straight or hooked-end bar lap splices, the latter had 8% and 9% greater strength after cracking, respectively, compared to that with continuous bars. This can be attributed to the higher reinforcement ratio at the midspan of the beams with bar lap splices, particularly that with hooked-end bars.

Benmokrane et al. tested FRP bars in concrete beams to study the effect of reinforcement ratio on a few parameters, such as ultimate capacities and failure modes [30]. In that study, it was concluded that the ultimate moment capacity increased by increasing the beam reinforcement ratio. However, there was a limitation to the maximum increased strength due to the concrete compressive failure strain. Moreover, the effect of reinforcement ratio on concrete beam damage was studied by Kattan and Voyiadjis, as their study showed that increasing reinforcement ratio decreased the damage in the experimentally tested beams [31]. Although the reinforcement ratio at the middle of the beams with lap splices was double the one with continuous bars, its influence was small, as can be seen in **Figure 10**. For example, at a deflection of 13 mm, the strengths of both the specimens with lap splices were about 280 kN while this parameter was 257 kN for the beam with continuous bars. The difference is 8%, which is small because in the beams with bar lap splices, GFRP bars were not continuous, and the reinforcement ratio was not twice in all parts of the beam.

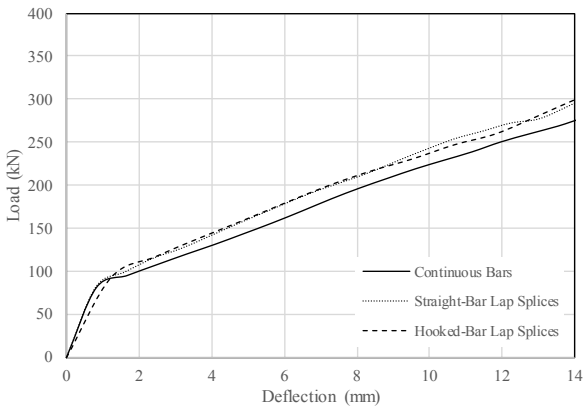

Figure 10. Load-deflection relationships of beams modelled with continuous vs. spliced bars.

3.2 Effect of bar diameter

As a second parameter investigated in this study, three different bar diameters (i.e., 20, 15, and 10 mm) were modeled in both beam reinforcement configurations, with straight and hooked-end bar lap splices. As shown in **Figure 11**, decreasing the bar diameter has an almost negligible effect on the beam's initial stiffness. However, considerable dif-

ferences in the flexural behaviour of the modelled beam with different bar diameters were observed after cracking. The magnitude of the applied load at the maximum attained midspan deflection of 14 and 22 mm for the beam modelled with a 10-mm bar diameter was smaller than half of that of the beam modelled with 20-mm diameter bars in both beam configurations, with straight and hooked-end bar lap splices, **Figure 11**, respectively.

A comparison between the results of section 3.1 and this section shows that the parameter that had an enormous effect on the strength of the specimens was the reinforcement ratio. For example, when the diameter of the GFRP bars was 15 mm, the reinforcement ratio was 2.25 times that of the beam with 10 mm bars. The former strength was 200 kN, while the latter was about 128 kN at a deflection of 12 mm in the beams with straight-end lap splices. The difference was 36%.

3.3 Effect of the number of bars

To study the effect of the number of GFRP bars on the behaviour of the modelled beams, the number of bars with 10 mm diameter was increased from 3 to 4 and 5 bars. Because of the relatively large width of the modelled beams, i.e., 300 mm, there was enough space to accommodate more than three bars. As can be seen in **Figure 12**, increasing the number of bars had almost no effect on the initial stiffness of the concrete beams. However, at the maximum attained midspan deflection of 14 mm, the beam modelled with five bars sustained an applied load that was about 13% and 33% more than the loads sustained by those modelled with four and three bars, respectively, all with straight-end bar lap splices. For the beams with hooked-end bar lap splices, at the maximum attained midspan deflection of 22 mm, the beam with five bars sustained applied load that also was about 13% and 33% more than the loads sustained by those modelled with four and three bars, respectively. The maximum attained beam midspan deflection values (i.e., 14 and 22 mm) of the beams modelled with straight and hooked-end bar lap splices, respectively, were determined from the referenced experimental study conducted by Nour et al. [24]. Similar results to section 3.2 were obtained in this section, which confirms the effect of increasing the reinforcement ratio along the entire length of the beam.

3.4 Effect of the length of lap splices

The length of the bar lap splices is one of the very important parameters that has been studied by a few numbers of researchers [32]. In addition, many design standards specify a minimum splice length that is mainly based on the bar diameter and other factors, e.g., bar end anchorage, bar surface configuration, etc. This study modelled 15 to 40 times the bar di-

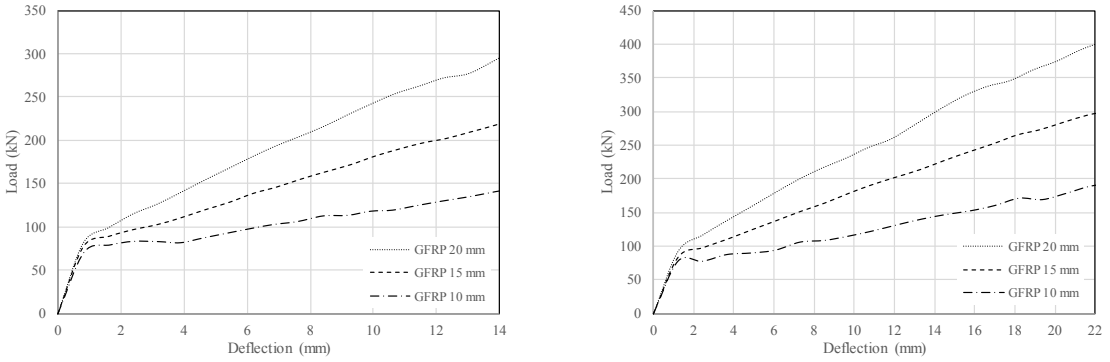

(a) Beams modelled with straight-end bar lap splices. (b) Beams modelled with hooked-end bar lap splices.

Figure 11. Load-deflection relationships of beams modelled with different bar diameters.

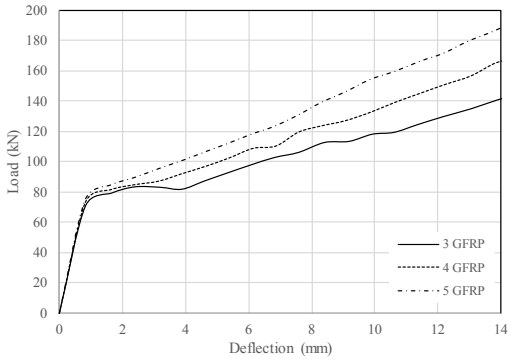

(a) Beams modelled with straight-end bar lap splices.

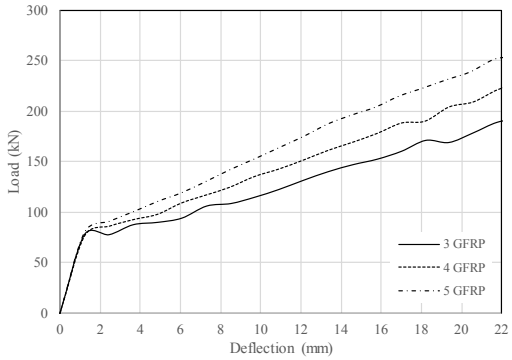

(b) Beams modelled with hooked-end bar lap splices.

Figure 12. Load-deflection relationships of beams modelled with different number of bars.

ameter lap splice lengths, i.e., 300, 550, and 800 mm. These splice lengths were calculated according to the CSA-S806-12 design standard [33] for straight and hooked-end bar lap splices, as per Nour et al. [24]. **Figure 13** illustrates the effect of increasing the splice length on the flexural behaviour of the beam in terms of its midspan deflections for beams modelled with straight and hooked-end bar lap splices, respectively. As shown in the figures, there was almost no measurable difference between the initial stiffnesses of the beams modelled with the three different splice lengths. However, at the maximum attained midspan deflection of 14 mm, the beam modelled with 800 mm splice length sustained applied load that was about 7% and 11% more than the loads sustained by those modelled with 550- and 300-mm splice lengths, respectively, all with straight-end bar lap splices. While for the beams with hooked-end bar lap splices, at the maximum attained midspan deflection of 22 mm, the beam modelled with 800 mm splice length sustained applied load that was about 5% and 10% more than the loads sustained by those modelled with 550- and 300-mm splice lengths, respectively. It became clear that various lengths of lap splices did not have a great effect on the strength of the beam. It proved that the minimum amount of reinforcement ratio along the beam defined the strength of the beam, whether the splices were straight or hooked.

3.5 Effect of bar material

To compare the behaviour of the concrete beams reinforced with bars made of different materials, beams were also modelled using conventional steel bars of the same diameter as the GFRP bars for both straight and hooked-end bar lap spliced beam configurations. As shown in **Figure 14**, the beams mod-

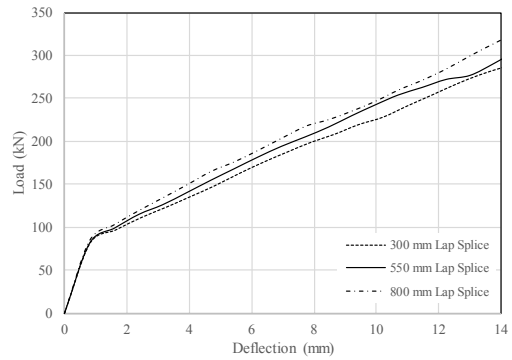

(a) Beams modelled with straight-end bar lap splices.

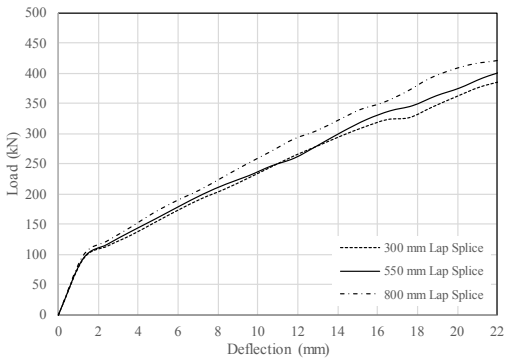

(b) Beams modelled with hooked-end bar lap splices.

Figure 13. Load-deflection relationships of beams modelled with different splice lengths.

elled with steel bars have higher stiffness, strength, and ductility than those modelled with GFRP bars. At the maximum attained midspan deflection of 14 mm, the beam modelled with steel bars sustained an applied load about 26% more than the beam modelled with GFRP bars, both with straight-end bar lap splices. While for the beam with hooked-end bar lap splices, at the maximum attained midspan deflection of 22 mm, the beam modelled with steel bars sustained an applied load that was about 14% more than that sustained by the beam modelled with GFRP bars. This also concurs with the results of an experimental study conducted by Szczech and Kotynia in which they investigated the bond strength of GFRP and steel reinforcement in concrete beams through pull-out tests, as they concluded that steel bars have stronger bond strength compared to GFRP bars having the same diameter and anchorage length [34].

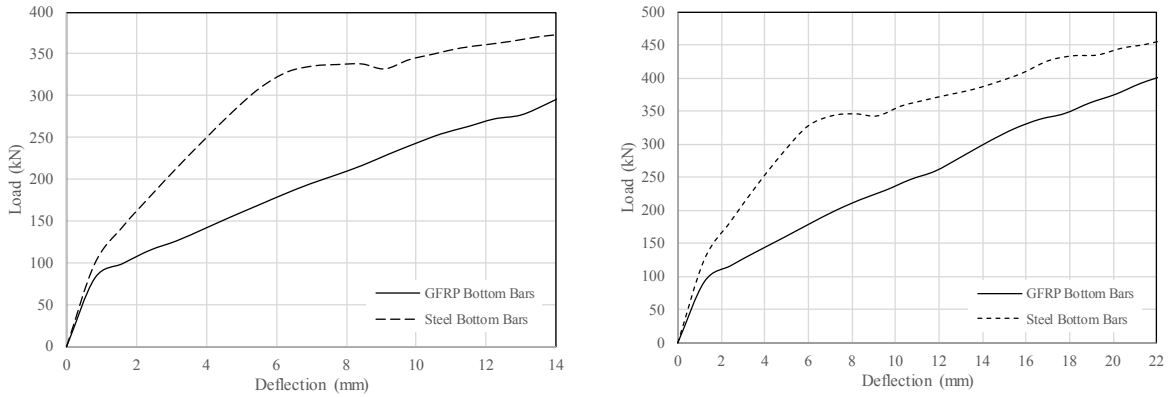

(a) Beams modelled with straight-end bar lap splices.

(b) Beams modelled with hooked-end bar lap splices.

Figure 14. Load-deflection relationships of beams modelled with GFRP and steel bars.

4. Conclusions

Due to the lack of research data on the performance of concrete beams reinforced with 180-degree hooked-end GFRP bars and having midspan bar lap splices, a numerical study involving three-dimensional FE modelling that is based on the experimental study carried out by Nour et al. [24] on four full-size beams that had straight, and hooked-end bar lap splices have been conducted. An extensive parametric study to investigate the effects of parameters such as bar continuity, bar diameter, number of bars, bar material and splice length is presented in this paper. The following conclusions have been drawn from the numerical analysis outcomes.

- Numerical simulation could accurately model concrete beams with straight or hooked-end bar lap splices. In terms of beam stiffness, flexural strength, and ductility, good agreement was achieved between the FE model predictions and the experimental results used to validate the models.
- By comparing load-deflection relationships of the beams modelled with spliced bars with those modelled with continuous bars, it is noticed that the initial stiffness of the continuous bar beam was greater than that of the beams modelled with spliced bars, either with straight or hooked-end bar lap splices. However, after cracking, beams with bar lap splices had greater ultimate flexural strength than those with continuous reinforcing bars.
- By changing the diameter of the GFRP bars (i.e., 20, 15, and 10 mm), it was seen that before cracking, the beams with different bar diameters behaved very similarly. However, after cracking, the magnitude of the applied load at the maximum attained midspan deflections of 14 and 22 mm for the beam modelled with a 10-mm bar diameter was less than half of that of the beam modelled with a 20-mm bar diameter in both beam configurations, with straight and hooked-end bar lap splices, respectively.
- Increasing the number of bars had almost no effect on the concrete beam's initial stiffness.

However, at the maximum attained midspan deflection, the beam modelled with five bars sustained an applied load that was about 13% and 33% more than that sustained by the beams modelled with four and three bars, respectively, for both straight and hooked-end bar lap splices beam configurations.

- Increasing the splice length from 300 to 550 and 800 mm had almost no measurable effect on the initial stiffness of the modelled concrete beams. However, at the maximum attained midspan deflection of 14 mm, the beam modelled with 800 mm splice length sustained applied load that was about 7% and 11% more than that sustained by the beams modelled with 550- and 300-mm splice lengths, respectively, all with straight-end bar lap splices. While for the beams with hooked-end bar lap splices, at the maximum attained midspan deflection of 22 mm, the beam modelled with 800 mm splice length sustained applied load that was about 5% and 10% more than that sustained by the beams modelled with 550- and 300-mm splice lengths, respectively.
- By substituting GFRP bars with steel bars, the beam flexural strength increased enormously, which is attributed to the reinforcing steel material's greater strength and elastic modulus than GFRP.

Author Contributions

Sara Mirzabagheri: Methodology, Validation, Formal analysis, Writing—Original Draft, Visualization.

Sam Salem: Conceptualization, Validation, Investigation, Resources, Writing—Review & Editing, Supervision, Project administration, Funding acquisition.

Conflict of Interest

The authors declare that there is no conflict of interest concerning the publication of this manuscript.

Data Availability Statement

The data that support the findings of this study are openly available in this article.

Funding

This research project was funded using a Discovery Grant awarded to the second author by the Natural Sciences and Engineering Research Council of Canada (NSERC).

References

[1] Long-term Performance of GFRP Reinforcement [Internet]. Texas Transportation Institute. Available from: https://rosap.ntl.bts.gov/view/dot/17628/dot_17628_DS1.pdf

[2] Ehsani, M.R., Saadatmanesh, H., Tao, S., 1996. Design recommendation for bond of GFRP rebars to concrete. Journal of Structural Engineering. 122(3), 247–254. DOI: https://doi.org/10.1061/(ASCE)0733-9445(1996)122:3(247)

[3] Morphy, R.D., 1999. Behaviour of fiber reinforced polymer (FRP) stirrups as shear reinforcement for concrete structures [Master's thesis]. Winnipeg: University of Manitoba.

[4] Yang, J.M., Min, K.H., Shin, H., et al., 2012. Effect of steel and synthetic fibers on flexural behaviour of high-strength concrete beams reinforced with FRP bars. Composites Part B Engineering. 43(3), 1077–1086. DOI: https://doi.org/10.1016/j.compositesb.2012.01.044

[5] Rehabilitation of Concrete Structures with CFRP Strips Glued into Slits [Internet]. Available from: https://citeseerx.ist.psu.edu/document?repid=rep1&type=pdf&doi=1175338445b942b34ee2f33f735605c02bf972ff

[6] Nanni, A., Alkhrdaji, T., Barker, M., et al. (editors), 1999. Overview of testing to failure program of a highway bridge strengthened with FRP composites. Proceeding of 4th International Symposium on Non-Metallic (FRP) Reinforcement for Concrete Structures (FRPRCS-4); 1999 Oct 31–Nov 5; Baltimore, MD.

[7] Wu, Z., Yuan, H., Hideki, Y., et al., 2001. Experimental/analytical study on interfacial fracture energy and fracture propagation along

FRP-concrete interface. ACI International. 201, 133–152.
DOI: https://doi.org/10.14359/10762

[8] Yao, J., Teng, J.G., Chen, J.F., 2004. Experimental study on FRP to concrete bonded joints. Composites Part B: Engineering. 36(2), 99–113.
DOI: https://doi.org/10.1016/j.compositesb.2004.06.001

[9] De Lorenzis, L., La Tegola, A., 2003. Analytical modeling of splitting bond failure for NSM FRP reinforcement in concrete. Fibre-reinforced polymer reinforcement for concrete structures. World Scientific Publishing: Singapore. pp. 975–984.

[10] Yuan, H., Teng, J.G., Seracino, R., et al., 2004. Full-range behavior of FRP-to concrete bonded joints. Engineering Structures. 26(5), 553–565.
DOI: https://doi.org/10.1016/j.engstruct.2003.11.006

[11] Sharaky, I.A., Torres, L., Comas, J., et al., 2014. Flexural response of reinforced concrete (RC) beams strengthened with near surface mounted (NSM) fibre reinforced polymer (FRP) bars. Composite Structures. 109, 8–22.
DOI: https://doi.org/10.1016/j.compstruct.2013.10.051

[12] Fillmore, B., Sadeghian, P., 2018. Contribution of longitudinal glass fiber-reinforced polymer bars in concrete cylinders under axial compression. Canadian Journal of Civil Engineering. 45, 458–468.
DOI: https://doi.org/10.1139/cjce-2017-0481

[13] Mirzabagheri, S., Tasnimi, A.A., Issa, F., 2018. Experimental and numerical study of reinforced concrete interior wide beam-column joints subjected to lateral load. Canadian Journal of Civil Engineering. 45(11), 947–957.
DOI: https://doi.org/10.1139/cjce-2018-0049

[14] Mirzabagheri, S., Tasnimi, A.A., 2019. Evaluation of CSA and ACI shear strength factor for RC roof wide and conventional beam-column joints. Ingegneria Sismica. 36(1).

[15] Yang, F., 2014. Deformation behaviour of beams reinforced with fibre reinforced polymer bars under bending and shear [Ph.D. thesis]. Sheffield: University of Sheffield.

[16] Stoner, J.G., 2015. Finite element modelling of GFRP reinforced concrete beams [Master's thesis]. Waterloo: University of Waterloo.

[17] Roudsari, S., Hamoush, S., Soleimani, S., et al., 2018. Analytical study of reinforced concrete beams strengthened by FRP bars subjected to impact loading conditions. arXiv preprint arXiv:1806.06929.
DOI: https://doi.org/10.48550/arXiv.1806.06929

[18] Elchalakani, M., Karrech, A., Dong, M., et al., 2018. Experiments and finite element analysis of GFRP reinforced geopolymer concrete rectangular columns subjected to concentric and eccentric axial loading, Structures. 14, 273–289.
DOI: https://doi.org/10.1016/j.istruc.2018.04.001

[19] Raza, A., Zaman Khan, Q.u., Ahmad, A., 2019. Numerical investigation of load-carrying capacity of GFRP-reinforced rectangular concrete members using CDP model in ABAQUS. Advances in Civil Engineering.
DOI: https://doi.org/10.1155/2019/1745341

[20] Aly, R., Benmokrane, B., Ebead, U., 2006. Tensile lap splicing of fiber-reinforced polymer reinforcing bars in concrete. ACI Structural Journal. 857–864.

[21] Esfahani, M.R., Rakhshanimehr, M., Mousavi, R., 2013. Bond strength of lap-spliced GFRP bars in concrete beams. Journal of Composites for Construction. 17(3), 314–323.
DOI: https://doi.org/10.1061/(ASCE)CC.1943-5614.0000359

[22] Wu, C., Hwang, H.J., Ma, G., 2022. Effect of stirrups on the bond behavior of lap spliced GFRP bars in concrete beams. Engineering Structures. 266, 114552.
DOI: https://doi.org/10.1016/j.engstruct.2022.114552

[23] Abbas, H., Elsanadedy, H., Alaoud, L., et al., 2023. Effect of confining stirrups and bar gap

in improving bond behavior of glass fiber reinforced polymer (GFRP) bar lap splices in RC beams. Construction and Building Materials. 365, 129943.
DOI: https://doi.org/10.1016/j.conbuildmat.2022.129943

[24] Nour, O., Salem, O., Mostafa, A., 2022. Experimental testing of GFRP-reinforced concrete beams with mid-span lap splices utilizing straight- and hooked-end bars. Lecture notes in civil engineering (LNCE). Springer: Cham.
DOI: https://doi.org/10.1007/978-3-031-09409-5_12

[25] ABAQUS 6.14: Analysis User's Guide [Internet]. Available from: https://www.academia.edu/28334906/Abaqus_Analysis_Users_Guide/

[26] Maekawa, K., Pimanmas, A., Okamura, H., 2003. Nonlinear mechanics of reinforced concrete. CRC Press: Boca Raton.

[27] Eurocode 2: Design of Concrete Structures-Part 1-2: General Rules- Structural Fire Design (EN 1992-1-2) [Internet]. European Standard. Available from: https://www.phd.eng.br/wp-content/uploads/2015/12/en.1992.1.2.2004.pdf

[28] Poliotti, M., Bairan, J.M., 2019. A new concrete plastic-damage model with an evolutive dilatancy parameter. Engineering Structures. 189, 541–549.
DOI: https://doi.org/10.1016/j.engstruct.2019.03.086

[29] Wosatko, A., Winnicki, A., Polak, M.A., et al., 2019. Role of dilatancy angle in plasticity-based models of concrete. Archives of Civil and Mechanical Engineering. 19(4), 1268–1283.
DOI: https://doi.org/10.1016/j.acme.2019.07.003

[30] Benmokrane, B., Theriault, M., Masmoudi, R., et al., 2003. Effect of reinforcement ratio on concrete members reinforced with FRP bars.

[31] Kattan, P.I., Voyiadjis, G.Z., 2007. Effect of reinforcement ratio on damage in reinforced concrete beams—A damage mechanics approach. Jordan Journal of Civil Engineering. 1(1), 73–82.

[32] El-Azab, A., Mohamed, H.M., 2014. Effect of tension lap splice on the behaviour of high strength concrete (HSC) beams. HBRC Journal. 10(3), 287–297.
DOI: https://doi.org/10.1016/j.hbrcj.2014.01.002

[33] Canadian Standard Association, 2012. Design and construction of building structures with fibre-reinforced polymers (CSA-S806-12). CSA Group: Mississauga, Ontario.

[34] Szczech, D., Kotynia, R., 2018. Beam bond tests of GFRP and steel reinforcement to concrete. Archives of Civil Engineering. 64(4), 243–256.
DOI: https://doi.org/10.2478/ace-2018-0072

Appendix

c	=	Stiffening parameter (0.4 for deformed bar, 0.2 for welded wire mesh)
F	=	Yield function
f_c	=	Compressive strength of concrete
f_t	=	Tensile strength of concrete
G	=	Flow potential
K_c	=	Ratio of second irreversible stress in the tensile meridian to this value in the compressive meridian
$\overline{p}$	=	Effective hydrostatic pressure
$\overline{q}$	=	Mises equivalent effective stress
$\overline{S}$	=	Deviatoric part of effective stress tensor
β	=	Strain rate factor
Ψ	=	Dilation angle measured in the p-q plane
$\in$	=	Eccentricity
ε	=	Strain
ε_c	=	Strain of concrete corresponding to
ε_{tu}	=	Cracking strain
σ_{b0}	=	Initial biaxial compressive yield stress
σ_c	=	Compressive stress
σ_{c0}	=	Initial uniaxial compressive yield stress
$\overline{\sigma}_c(\tilde{\varepsilon}_c^{pl})$	=	Effective uniaxial cohesion compressive stress
$\hat{\overline{\sigma}}_{max}$	=	Algebraically maximum effective stress
σ_t	=	Tensile stress
σ_{t0}	=	Uniaxial tensile stress at failure